Thermoelectric transport through Majorana bound states and violation of Wiedemann-Franz law

J. P. Ramos-Andrade,[1,2,*] O. Ávalos-Ovando,[2] P. A. Orellana,[1] and S. E. Ulloa[2]

[1]*Departamento de Física, Universidad Técnica Federico Santa María, Casilla 110 V, Valparaíso, Chile*

[2]*Department of Physics and Astronomy, and Nanoscale and Quantum Phenomena Institute, Ohio University, Athens, Ohio 45701–2979, USA*

(Received 5 August 2016; published 20 October 2016)

We study features of thermoelectric transport through a one-dimensional topological system model hosting Majorana bound states (MBSs) at its ends. We describe the behavior of the Seebeck coefficient and the ZT figure of merit for two configurations between the MBS and normal current leads. We find an important violation of the Wiedemann-Franz law in one of these geometries, leading to sizable values of the thermoelectric efficiency over a narrow window in chemical potential away from neutrality. These findings could lead to interesting thermoelectric-based MBS detection devices, via measurements of the Seebeck coefficient and figure of merit.

DOI: 10.1103/PhysRevB.94.155436

I. INTRODUCTION

A new kind of fermionic quasiparticle has been studied in the context of condensed matter in recent years, with its principal feature being that it is its own antiparticle. These Majorana fermions (MFs), first predicted by E. Majorana [1], have other interesting properties such as satisfying non-Abelian statistics and are therefore of interest in quantum computation implementations [2,3]. These quasiparticles appear in systems with particle-hole symmetry as zero-energy excitations and are predicted to be found at the ends of a one-dimensional (1D) semiconductor nanowire with spin-orbit interaction (SOI) in a magnetic field and proximitized by an adjacent superconductor [4,5]. Such Majorana states may also appear in other systems as in a vortex of a p-wave superconductor [6], on the surface of a topological insulator [7], and at the ends of a chain of magnetic impurities on a superconducting surface [8,9]. The Majorana bound states (MBSs) at the end of such a wire/chain system can be seen as the implementation of a Kitaev chain [10]. Mourik *et al.* [11] reported the first observation of Majorana signatures in a semiconductor-superconductor nanowire, built of InSb (indium antimonide) and NbTiN (niobium titanium nitride), with several others groups reporting zero-bias conductance peaks in similar hybrid devices [12–15]. MBS pairs are predicted to interact with a coupling strength ε_M proportional to $\exp[-\mathcal{L}/\xi]$, where $\mathcal{L}$ is the wire length and ξ is the superconducting coherence length. Recent experimental work has probed this dependence of ε_M in wire length, verifying expectation[16].

Moreover, there is a great deal of interest in the thermoelectricity of nanostructures [17–19]. When a thermal bias is applied across a system, a quantity of interest is the thermoelectric energy-conversion efficiency, characterized by the dimensionless figure of merit ZT, which involves the Seebeck coefficient, as well as the ratio of thermal and electrical conductances [20]. A way to improve ZT is to overcome the Wiedemann-Franz (WF) law, which sets the ratio $\kappa/\mathcal{G}T = \ell_0 \equiv$ constant in all systems, where $\mathcal{G}$ is the electrical conductance, κ the thermal conductance, T the background temperature, and $\ell_0 = (\pi^3/3)(k_B/e)^2$ the Lorenz number [21]. Although macroscopic materials have shown to generally follow the WF law, nanostructured systems have proved to be very good thermoconverters, as they are able to overcome that restriction [22]. Thermoelectric efficient devices have been proposed in systems such as molecular junctions [23,24], quantum dots [25], and topological insulators [26]. Thermal detection of Majorana states in topological superconductors has also been proposed [27]. Even though several Majorana detection setups have been realized [8,11–15], much less attention has been directed to thermoelectric-based detection devices. Different thermoelectric setups with Majorana nanowires and/or connected quantum dots have been considered, where thermal biases are applied across the normal leads [28,29] or across normal lead-superconductor setups [30,31]. These systems are found to exhibit signatures of MBSs through measurements of the Seebeck coefficient as the energy of the level in the dot varies, even in a weak-coupling regime.

In this work we study the thermoelectrical properties of an MBS system coupled to two normal leads in the presence of a thermal bias. The system between the leads is considered a 1D topological superconductor nanowire containing the MBS at its ends, which under suitable conditions could represent any time-reversal symmetry-breaking topological superconductor, such as a Kitaev chain [10]. We model the nanowire with an effective low-energy Hamiltonian hosting two MBSs, γ_1 and γ_2, coupled between them with a strength ε_M (assumed known). Using a Green's function formalism, we study the thermoelectric transport across the system, in two configurations: (i) when both MBSs are connected to the leads and (ii) when only one MBS is connected to the leads. The first configuration was discussed in Ref. [28] for the case of zero chemical potential ($\mu = 0$) in contacts. Our findings agree with their results and go further as the chemical potential varies. We find a small Seebeck coefficient and vanishing small ZT over a broad range of chemical potential and coupling ε_M at typical low experimental temperatures. On the other hand, we find a sizable violation of the WF law for the second configuration, which leads to large values of thermoelectric efficiency, as measured by the figure of merit. We also find an ε_M-independent behavior of the thermal quantities with large ε_M values for the same configuration. These features should be accessible in experiments and may help provide additional insights into the presence of behavior of MBSs in nanowire systems.

This paper is arranged as follows: Section II presents the model and Hamiltonian used for obtaining the thermoelectric

*juan.ramosa@usm.cl

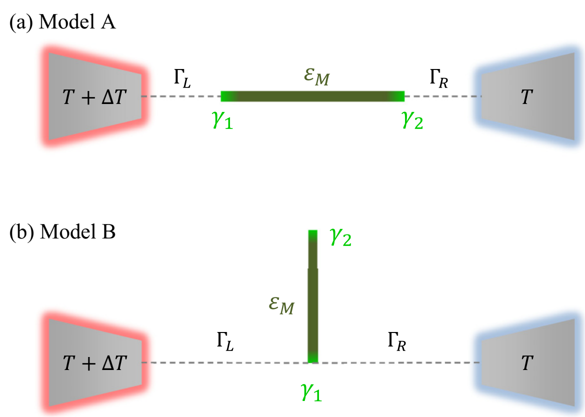

FIG. 1. Model setup of a 1D topological superconductor nanowire hosting an MBS at both ends, connected to two metallic leads at different temperatures. (a) Each MBS is coupled to its nearest lead; (b) only one MBS is coupled to both leads simultaneously.

quantities. Section III reports the results and discussion; and finally, concluding remarks are given in Sec. IV.

II. MODEL

We consider a two-MBS system, each located at the ends of the nanowire and coupled to two metallic leads in two different configurations, as shown schematically in Fig. 1. The left lead L is kept at temperature $T+\Delta T$ and the right lead R at temperature T, thus providing a temperature gradient ΔT. We describe the system with a noninteracting Anderson Hamiltonian within the second quantization framework and consider it spin-independent because of the strong Zeeman effect due to the applied magnetic field. The Hamiltonian is given by [28]

$$H = H_{\text{leads}} + H_{\text{leads-MBS}} + H_{\text{MBS}}\,, \tag{1}$$

where H_{leads} describes the current leads, $H_{\text{leads-MBS}}$ the coupling between the leads and the MBS, and H_{MBS} the isolated MBSs. Each of them is given by

$$H_{\text{leads}} = \sum_{\alpha,k} \varepsilon_{\alpha,k} c^{\dagger}_{\alpha,k} c_{\alpha,k}, \tag{2}$$

$$H_{\text{MBS}} = i\varepsilon_M \gamma_1\gamma_2, \tag{3}$$

$$H_{\text{leads-MBS}} = \sum_{\alpha,k} t_{\alpha,\beta}\gamma_\beta c_{\alpha,k} + t^*_{\alpha,\beta} c^{\dagger}_{\alpha,k}\gamma_\beta, \tag{4}$$

where $c^{\dagger}_{\alpha,k}$ ($c_{\alpha,k}$) creates (annihilates) an electron of momentum k in lead $\alpha = L,R$, and γ_β creates one of the two MBSs ($\beta = 1,2$) and satisfies both $\{\gamma_\beta,\gamma_{\beta'}\} = 2\delta_{\beta,\beta'}$ and $\gamma_\beta = \gamma_\beta^\dagger$, i.e., an MBS is its own antiparticle. ε_M is the coupling between the two MBSs due to a finite length of the wire. The terms $t_{\alpha,\beta}$ are the tunneling hoppings between lead α and MBS β. For the two models shown in Fig. 1, the upper and lower panels consider $t_{L,1} = t_{R,2} \neq 0$ and $t_{L,1} = t_{R,1} \neq 0$, respectively, with others vanishing.

We obtain the transmission probability across the leads by using the Green's function formalism. In the linear response regime, we can obtain the transmission by means of the Fischer-Lee relation, given by

$$\mathcal{T}(\varepsilon) = \text{Tr}[\tilde{\Gamma}_L \tilde{G}^a(\varepsilon)\tilde{\Gamma}_R \tilde{G}^r(\varepsilon)], \tag{5}$$

with ε the energy of the electron tunneling from L to R, $\tilde{\Gamma}_\alpha$ being the coupling matrix of the lead α and $\tilde{G}^r(\varepsilon)$ [$\tilde{G}^a(\varepsilon)$] the retarded [advanced] Green's function matrix given by

$$\tilde{G}^r(\varepsilon) = \begin{pmatrix} \langle\langle\gamma_1,\gamma_1\rangle\rangle_\varepsilon & \langle\langle\gamma_1,\gamma_2\rangle\rangle_\varepsilon \\ \langle\langle\gamma_2,\gamma_1\rangle\rangle_\varepsilon & \langle\langle\gamma_2,\gamma_2\rangle\rangle_\varepsilon \end{pmatrix}, \tag{6}$$

where $\langle\langle A,B\rangle\rangle_\varepsilon$ denotes the Green's function between operator A and operator B in the energy domain and $G^a(\varepsilon) = [G^r(\varepsilon)]^\dagger$. We find the transmission coefficients for the two setups shown in Fig. 1, namely, models A and B, in what follows. These transmission expressions are $\mathcal{T}_{\text{A}}(\varepsilon)$ for model A and $\mathcal{T}_{\text{B}}(\varepsilon)$ for model B are and given by [32,33]

$$\mathcal{T}_{\text{A}}(\varepsilon) = \frac{4\Gamma^2\left(\varepsilon^2+\varepsilon_M^2+4\Gamma^2\right)}{(\varepsilon^2+4\Gamma^2)^2+\varepsilon_M^2\left(\varepsilon_M^2-2(\varepsilon^2-4\Gamma^2)\right)}, \tag{7}$$

$$\mathcal{T}_{\text{B}}(\varepsilon) = \frac{4\varepsilon^2\Gamma^2}{[(\varepsilon+\varepsilon_M)(\varepsilon-\varepsilon_M)]^2+4\varepsilon^2\Gamma^2}, \tag{8}$$

where Γ is the energy-independent coupling strength between the nanowire and the leads for the symmetric case in the wide band limit, where $t_{\alpha,\beta} \equiv t_0$ for all nonvanishing cases, and $\Gamma = \pi|t_0|^2\rho_0$, ρ_0 being the contact density of states.

As for thermoelectric quantities, we consider the system in the linear response regime, with a temperature difference ΔT between the two leads. In this scenario we can write the charge and heat current, I_{charge} and I_{heat}, respectively, in terms of a potential difference ΔV as [34]

$$I_{\text{charge}} = -e^2L_0\Delta V + \frac{e}{T}L_1\Delta T, \tag{9}$$

$$I_{\text{heat}} = eL_1\Delta V - \frac{1}{T}L_2\Delta T, \tag{10}$$

where e is the electron charge and

$$L_n(\mu) = \frac{1}{h}\int\left(-\frac{\partial \bar{f}(\varepsilon,\mu)}{\partial\varepsilon}\right)(\varepsilon-\mu)^n\mathcal{T}(\varepsilon)d\varepsilon, \tag{11}$$

where μ and $\bar{f}(\varepsilon,\mu)$ are the Fermi energy and Fermi distribution function, respectively, and h the Planck constant. The Seebeck coefficient S (or thermopower) relates the temperature difference ΔT and the potential difference ΔV caused when the charge current vanishes:

$$S(\mu) = -\frac{\Delta V}{\Delta T} = -\frac{1}{e\,T}\frac{L_1}{L_0}. \tag{12}$$

The electrical conductance $\mathcal{G}(\mu)$ and thermal conductance $\kappa(\mu)$ are defined as the ratio between the charge current and the potential difference when ΔT vanishes for the first and as the ratio between the heat current and the temperature gradient when the charge current vanishes for the latter. From Eqs. (9) and (10), both conductances are given by

$$\mathcal{G}(\mu) = -\frac{I_{\text{charge}}}{\Delta V} = e^2L_0, \tag{13}$$

$$\kappa(\mu) = -\frac{I_{\text{heat}}}{\Delta T} = \frac{1}{T}\left(L_2 - \frac{L_1^2}{L_0}\right). \tag{14}$$

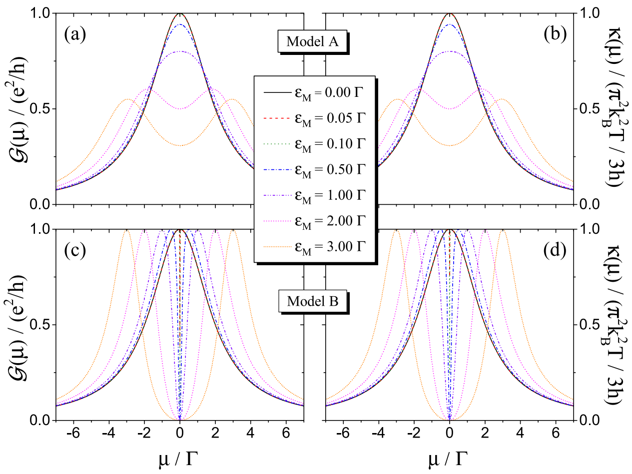

FIG. 2. (a, c) Electrical and (b, d) thermal conductances, both as a function of the Fermi energy μ. (a) and (b) correspond to model A in Fig. 1; (c) and (d), to model B.

Equation (14) considers only the electronic contribution to the thermal conductance; It assumes that the phononic contribution is negligible in the low-temperature regime (few kelvins) typical of the systems.

In order to quantify the efficiency of our MBS thermoelectric setups, we calculate the dimensionless figure of merit ZT,

$$ZT = \frac{S^2 \mathcal{G} T}{\kappa}, \tag{15}$$

as a function of the structure parameters.

III. RESULTS

A. Electrical and thermal conductance

In what follows we assume a background temperature of $T = 10$ K, well below typical superconductor critical temperatures [35]. We use Γ as a useful energy scale and set it to a characteristic experimental value, $\Gamma = 10$ meV, which leads to $k_B T \sim 10^{-1}\Gamma$, where k_B is the Boltzmann constant.

For the two setups shown in Fig. 1, models A and B, Fig. 2 shows the electrical conductance $\mathcal{G}$ and thermal conductance κ, in units of e^2/h and $\pi^2 k_B^2 T/3h$, respectively. Figures 2(a) and 2(b) show $\mathcal{G}$ and κ for model A, and Figs. 2(c) and 2(d) show $\mathcal{G}$ and κ for model B. In both models, the conductance reaches the maximum value $\mathcal{G}(\mu = 0) = e^2/h$ when the overlapping parameter ε_M between the two MBSs vanishes. The maximum $\mathcal{G}$ occurs whenever the chemical potential of the leads is resonant with the MBSs, as shown by solid black lines. The nonvanishing conductance signals the presence and entanglement of the MBSs at both ends, differentiating this regime from ordinary fermionic uncoupled modes expected to yield zero conductance. For model A when the ε_M is turned on, such that $0 < \varepsilon_M \lesssim k_B T$, the conductance shows the same behavior, as the central resonance cannot discern the MBS splitting and yields the same maximum magnitude located at $\mu \approx 0$. When $\varepsilon_M \gtrsim k_B T$, there is first a drop in amplitude in the conductance and then, after $\varepsilon_M \sim \Gamma$, a clear splitting of the central resonance. For model B, however, the central resonance is split into a central narrow dip at $\mu = 0$ and two side peaks at $\pm\varepsilon_M$, which reach the same magnitude $\mathcal{G}(\mu = \pm\varepsilon_M) = e^2/h$ in this symmetric coupling case, $\Gamma_L = \Gamma_R = \Gamma$. The splitting of the central resonance into two side peaks is very evident for $\varepsilon_M \gtrsim \Gamma$, with a broad 0 near $\mu = 0$. Note that both electrical and thermal conductances show the same qualitative behavior, except for a very subtle difference close to the antiresonance located at $\mu = 0$, as will be seen later.

Similar characteristics of the electrical conductance have been discussed in Ref. [36], as a function of the wire length $\mathcal{L}$. By comparison, we can observe that a large (short) $\mathcal{L}$ means a weak (strong) MBS overlap ε_M in our model, as one would expect from $\varepsilon_M \propto \exp[-\mathcal{L}/\xi]$, where ξ is the superconducting coherence length.

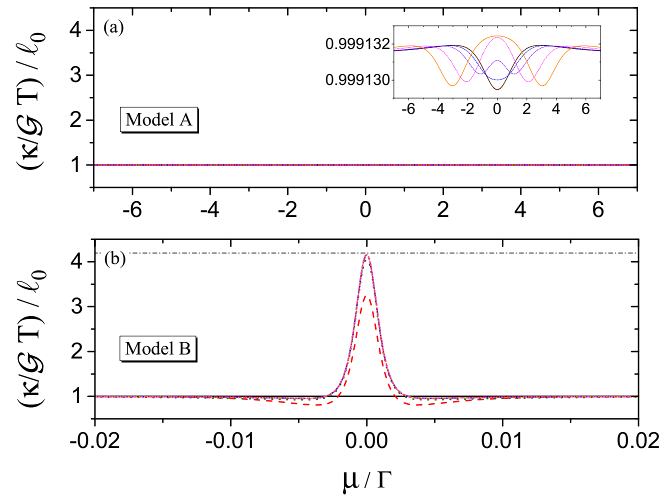

FIG. 3. Wiedemann-Franz law ratio, in units of the Lorenz number ℓ_0, for (a) model A and (b) model B in Fig. 1. The horizontal dotted-dashed gray line corresponds to the universal maximum value of 4.19 ℓ_0 [23].

B. Wiedemann-Franz law

Let us now explore the fulfillment of the WF law in both geometries by plotting the ratio $\kappa(\mu)/\mathcal{G}(\mu)T$ in Fig. 3(a) for model A and in Fig. 3(b) for model B, in units of the Lorenz number ℓ_0. For model A we observe a near-negligible violation of this law, as the $\kappa/\mathcal{G}T$ ratio is a constant up to the sixth decimal place. Note that $\mathcal{G}(\mu)T > \kappa(\mu)$ (in ℓ_0 units) is always fulfilled for any ε_M, and only the shape of the curves changes for $\varepsilon_M \lesssim \Gamma$ and $\varepsilon_M \gtrsim \Gamma$, as shown in Fig. 3(a). We emphasize that although this deviation from WF is small, it is well within the numerical accuracy of the calculation. For model B, on the other hand, the WF law is fulfilled for $\varepsilon_M = 0$, but for any $\varepsilon_M \neq 0$, the violation of the law is observed in a narrow range of μ, rising rapidly to the maximum value $\sim 4.19\ell_0$ for $\varepsilon_M \gtrsim k_B T$ at $\mu = 0$, as shown in Fig. 3(b). This phenomenon is a consequence of the antiresonance in the conductance, similar to those reported in molecules [23] and quantum dots [37]. This drastic violation of the WF law has not been reported before for systems hosting MBSs.

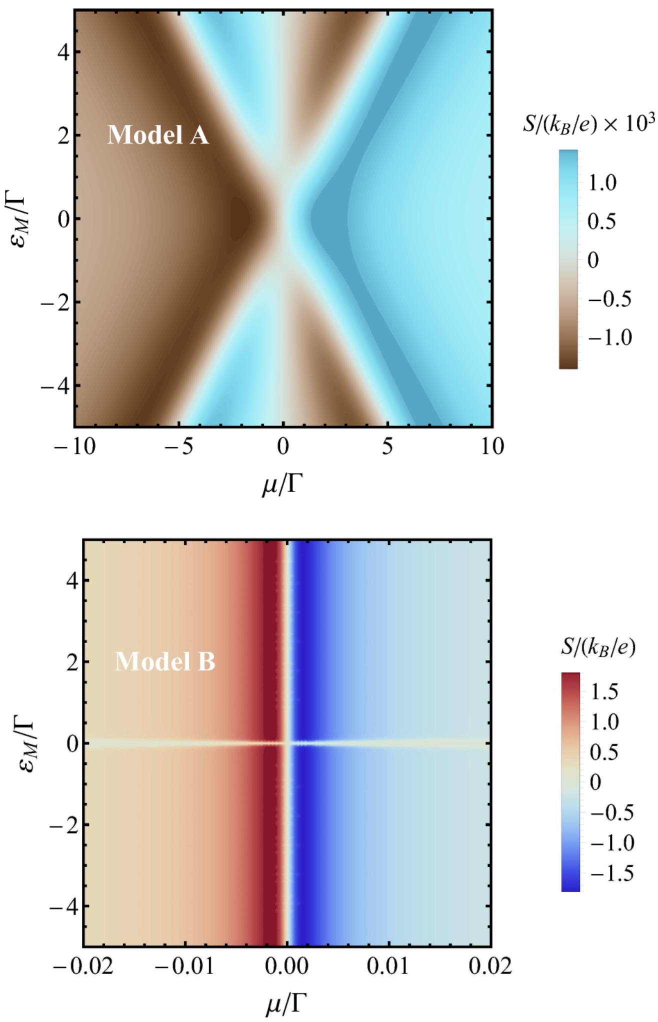

FIG. 4. Seebeck coefficient as a function of μ and ε_M. Upper and lower panels refer to model A and model B in Fig. 2, respectively. Note that S in model B can be three orders of magnitude larger than in model A geometry.

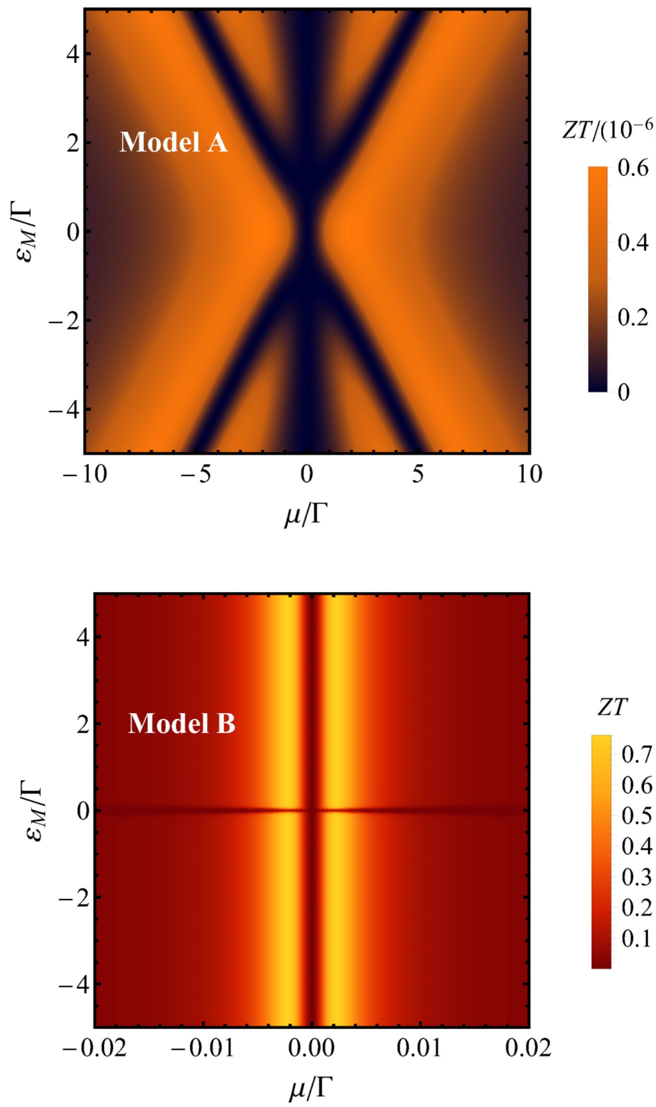

FIG. 5. ZT as a function of μ and ε_M. Upper and lower panels refer to model A and model B in Fig. 2, respectively. Note the sizable ZT in model B over the window $\Delta\mu \sim 0.002\Gamma \sim 20\ \mu$eV.

C. Thermoelectric efficiency

In order to quantify the thermoelectric efficiency of the two geometries, we plot the Seebeck coefficient (S) and figure of merit (ZT) in Figs. 4 and 5, respectively. These figures display the vanishing of S and ZT at $\mu = 0$, independent of the ε_M values [$S(\mu = 0) = ZT(\mu = 0) = 0$]. The sign of S with respect to μ depends on the ε_M value for model A, so that for $\mu \leq 0$ we get $S(\mu) \leq 0$ with $|\varepsilon_M| \leq \Gamma$, but for $|\varepsilon_M| > \Gamma$, S changes the sign of μ. A similar behavior can be seen for $\mu \geq 0$. On the other hand, in the lower panel in Fig. 4 (model B) the sign of S is essentially independent of ε_M, so that $\mu/S(\mu) \leq 0$ is always obtained, regardless of μ and ε_M. Note, however, that $S = 0$ for $\mu = 0$ and/or $\varepsilon_M = 0$, in sharp contrast to the behavior of model A. Besides, the ε_M gap shown around $\varepsilon_M = 0$ is proportional to the temperature (not shown). We propose to use the measurement of these features as a signature of the presence of MBSs.

From the upper panel in Fig. 5, we can easily see that model A is not thermoelectrically efficient, since $ZT \to 0$ ($\sim 10^{-7}$) over the entire parameter domain. In contrast, the lower panel in Fig. 5, for model B, shows that the system can be considered thermoelectrically efficient, as ZT is close to unity at least in two narrow μ ranges near 0. It is interesting that the high ZT value is independent of ε_M for $|\varepsilon_M| \gtrsim k_B T$.

IV. CONCLUSIONS

We have studied the thermoelectric transport through a nanowire hosting MBSs when a temperature gradient is applied. We find that when only one end of the nanowire is connected to normal metal leads sustaining a thermal gradient, the ZT figure of merit approaches 1 for small deviations of the chemical potencial away from 0. Although experiments to explore this phenomenon would require control of $\Delta\mu \sim 20\ \mu$eV, they would provide unique signatures of MBS in these systems.

ACKNOWLEDGMENTS

J.P.R.-A. is grateful for the hospitality of Ohio University and the funding of scholarship CONICYT-Chile No.

21141034. P.A.O. acknowledges support from FONDECYT Grant No. 1140571 and CONICYT ACT 1204. S.E.U. and O.Á.-O. acknowledge support from NSF Grant No. DMR 1508325.

[1] E. Majorana, Nuovo Cimento **14**, 171 (1937).
[2] J. Alicea, Nature **531**, 177 (2016).
[3] J. Alicea, Y. Oreg, G. Refael, F. von Oppen, and M. P. A. Fisher, Nat. Phys. **7**, 412 (2011).
[4] R. M. Lutchyn, J. D. Sau, and S. Das Sarma, Phys. Rev. Lett. **105**, 077001 (2010).
[5] Y. Oreg, G. Refael, and F. von Oppen, Phys. Rev. Lett. **105**, 177002 (2010).
[6] D. A. Ivanov, Phys. Rev. Lett. **86**, 268 (2001).
[7] L. Fu and C. L. Kane, Phys. Rev. Lett. **100**, 096407 (2008).
[8] S. Nadj-Perge, I. K. Drozdov, J. Li, H. Chen, S. Jeon, J. Seo, A. H. MacDonald, B. A. Bernevig, and A. Yazdani, Science **346**, 602 (2014).
[9] M. Ruby, F. Pientka, Y. Peng, F. von Oppen, B. W. Heinrich, and K. J. Franke, Phys. Rev. Lett. **115**, 197204 (2015).
[10] A. Y. Kitaev, Phys. Usp. **44**, 131 (2001).
[11] V. Mourik, K. Zuo, S. M. Frolov, S. R. Plissard, E. P. A. M. Bakkers, and L. P. Kouwenhoven, Science **336**, 1003 (2012).
[12] M. T. Deng, C. L. Yu, G. Y. Huang, M. Larsson, P. Caroff, and H. Q. Xu, Nano Lett. **12**, 6414 (2012).
[13] A. Das, Y. Ronen, Y. Most, Y. Oreg, M. Heiblum, and H. Shtrikman, Nat. Phys. **8**, 887 (2012).
[14] H. O. H. Churchill, V. Fatemi, K. Grove-Rasmussen, M. T. Deng, P. Caroff, H. Q. Xu, and C. M. Marcus, Phys. Rev. B **87**, 241401(R) (2013).
[15] L. P. Rokhinson, X. Liu, and J. K. Furdyna, Nat. Phys. **8**, 795 (2012).
[16] S. M. Albrecht, A. P. Higginbotham, M. Madsen, F. Kuemmeth, T. S. Jespersen, J. Nygård, P. Krogstrup, and C. M. Marcus, Nature **531**, 206 (2016).
[17] Y. Dubi and M. Di Ventra, Rev. Mod. Phys. **83**, 131 (2011).
[18] G. E. W. Bauer, E. Saitoh, and B. J. van Wees, Nat. Mater. **11**, 391 (2012).
[19] D. Sánchez and H. Linke, New J. Phys. **16**, 110201 (2014).
[20] H. Goldsmid, *Thermoelectric Refrigeration* (Plenum Press, New York, 1964).
[21] R. Franz and G. Wiedemann, Ann. Phys. (Berlin) **165**, 497 (1853).
[22] C. J. Vineis, A. Shakouri, A. Majumdar, and M. G. Kanatzidis, Adv. Mater. **22**, 3970 (2010).
[23] J. P. Bergfield and C. A. Stafford, Nano Lett. **9**, 3072 (2009).
[24] P. Reddy, S.-Y. Jang, R. A. Segalman, and A. Majumdar, Science **315**, 1568 (2007).
[25] P. Trocha and J. Barnaś, Phys. Rev. B **85**, 085408 (2012).
[26] O. A. Tretiakov, Ar. Abanov, and J. Sinova, Appl. Phys. Lett. **99**, 113110 (2011).
[27] N. V. Gnezdilov, M. Diez, M. J. Pacholski, and C. W. J. Beenakker, Phys. Rev. B **94**, 115415 (2016).
[28] R. López, M. Lee, L. Serra, and J. S. Lim, Phys. Rev. B **89**, 205418 (2014).
[29] H. Khim, R. López, J. S. Lim, and M. Lee, Eur. Phys. J. B **88**, 151 (2015).
[30] M. Leijnse, New J. Phys. **16**, 015029 (2014).
[31] S. Valentini, R. Fazio, V. Giovannetti, and F. Taddei, Phys. Rev. B **91**, 045430 (2015).
[32] J. S. Lim, R. López, and L. Serra, New J. Phys. **14**, 083020 (2012).
[33] K. Flensberg, Phys. Rev. B **82**, 180516(R) (2010).
[34] J. M. Ziman, *Electrons and Phonons: The Theory of Transport Phenomena in Solids* (Oxford University Press, Oxford, UK, 1960).
[35] J. Nagamatsu, N. Nakagawa, T. Muranaka, Y. Zenitani, and J. Akimitsu, Nature **410**, 63 (2001).
[36] B. H. Wu and J. C. Cao, Phys. Rev. B **85**, 085415 (2012).
[37] G. Gómez-Silva, O. Ávalos-Ovando, M. L. Ladrón de Guevara, and P. A. Orellana, J. Appl. Phys. **111**, 053704 (2012).